

# Non-contact *in situ* microwave material measurements for high temperature process monitoring

Cite as: Rev. Sci. Instrum. **90**, 034702 (2019); <https://doi.org/10.1063/1.5079796>

Submitted: 03 November 2018 . Accepted: 09 February 2019 . Published Online: 04 March 2019

Balamurugan T. Sivaprakasam , C. V. Krishnamurthy , and Kavitha Arunachalam 



View Online



Export Citation



CrossMark

## ARTICLES YOU MAY BE INTERESTED IN

[A novel 3D printed radial collimator for x-ray diffraction](#)

Review of Scientific Instruments **90**, 035102 (2019); <https://doi.org/10.1063/1.5063520>

[Self-forming mechanisms of sub-micro-/nanotips with controlled end geometry by membrane confined electrochemical turning technique](#)

Review of Scientific Instruments **90**, 035101 (2019); <https://doi.org/10.1063/1.5081480>

[Phase-sensitive dynamic susceptibility setup for measurements in pulsed magnetic fields](#)

Review of Scientific Instruments **90**, 033901 (2019); <https://doi.org/10.1063/1.5046475>



**JANIS**

**Janis Dilution Refrigerators & Helium-3 Cryostats for Sub-Kelvin SPM**

Click here for more info [www.janis.com/UHV-ULT-SPM.aspx](http://www.janis.com/UHV-ULT-SPM.aspx)

# Non-contact *in situ* microwave material measurements for high temperature process monitoring

Cite as: Rev. Sci. Instrum. 90, 034702 (2019); doi: 10.1063/1.5079796

Submitted: 3 November 2018 • Accepted: 9 February 2019 •

Published Online: 4 March 2019



View Online



Export Citation



CrossMark

Balamurugan T. Sivaprakasam,<sup>1</sup>  C. V. Krishnamurthy,<sup>2</sup>  and Kavitha Arunachalam<sup>1,a)</sup> 

## AFFILIATIONS

<sup>1</sup>Department of Engineering Design, Indian Institute of Technology Madras, Chennai 600036, India

<sup>2</sup>Department of Physics, Indian Institute of Technology Madras, Chennai 600036, India

<sup>a)</sup>akavitha@iitm.ac.in

## ABSTRACT

Non-contact real time microwave measurement and signal analysis techniques to extract high temperature material parameters from the mono-static reflections gathered by a compact air cooled corrugated horn are presented in this work. Non-contact *in situ* microwave measurements gathered over 20–24 GHz inside a closed furnace were processed to identify the thermodynamic phase change temperature of metal and glass melts. The melting point of aluminum alloy and glass transition of a borosilicate glass matrix extracted from the time gated and processed microwave measurements were in good agreement with differential scanning calorimetry measurements. Thus, the ability to measure high temperature material process parameters using non-contact microwave measurements is demonstrated.

Published under license by AIP Publishing. <https://doi.org/10.1063/1.5079796>

## I. INTRODUCTION

Real time monitoring of material parameters at high temperatures is essential for production and quality control in chemical, petroleum, ceramic, polymer, and food processing industries. The use of furnace in industry varies depending on the process such as agitation, aeration, emulsion, slurry formation, high temperature foaming, and curing. High temperature monitoring of molten solids is conventionally carried out using thermo wells in contact with the furnace contents. Alternate techniques reported in the literature primarily measure the material level inside the industrial vessel.<sup>1–4</sup> Boehmer and Smith<sup>1</sup> demonstrated an ultrasound sensor mounted inside the liquid sodium vessel for continuous measurement of the sodium level in a fast breeder reactor. Contact type acoustic sensing was proposed for measurement of the level of molten glass inside the furnace using a buffer rod immersed in the glass melt for guiding the wave<sup>2</sup> and mechanical properties<sup>5</sup> of metals using the respective metallic waveguide. Air coupled ultrasound sensors at a high

operating frequency suffer from signal attenuation when operated in pulse echo mode.<sup>6</sup> Pitch catch and transmission modes were proposed to reduce the impact of attenuation but were not demonstrated for high temperature material measurements in a furnace. The ability to measure temperature and emissivity of molten glass was demonstrated using a millimeter wave open ended corrugated dielectric waveguide operating in contact mode at 137 GHz.<sup>3</sup> The signal received for varying dielectric waveguide immersion lengths in the molten mass was related to the material state. Material and vapour deposition on the waveguide was reported to influence the measurements when exposed for long duration. Furthermore, the receiver for gathering the thermal emission is very sensitive to variation in ambient noise and temperature and noise temperature of the receiver electronics. Thus, it is challenging to deploy this technique in an industrial environment. Non-contact microwave measurements over 8–12 GHz using a regular horn and vector network analyzer (VNA) demonstrated the ability to measure the displacement in the level of molten glass with sub-millimeter accuracy.<sup>4</sup> Microwave reflections

recorded in a glass furnace with a wide opening were analyzed using the interferometry technique to measure the differential change in the level of the molten glass and not the absolute level.<sup>4</sup> Furthermore, as this technique is based on the interferometry principle, it has ambiguity in measuring displacement more than half wavelength. Finally, the proposed signal processing technique<sup>4</sup> does not yield high temperature material properties such as melting point and glass transition temperatures.

Prior work reported in the literature clearly indicates limited high temperature non-contact sensors for *in situ* measurement of high temperature material process parameters. Microwave based remote sensing is well suited for non-contact and non-destructive material evaluation<sup>7</sup> and long range measurement in a high temperature environment as they are not significantly influenced by temperature and pressure variations. Metal horn antennas commonly used for non-contact industrial level gauging have a relatively high side lobe level and asymmetric beam pattern in the vertical and horizontal illumination planes.<sup>8</sup> Dielectric rod antennas (8.5–10.5 GHz) reported for level measurement have a low side lobe level but limited operating temperature (<200 °C).<sup>9</sup> A compact air cooled corrugated metal horn operating at 22 GHz center frequency with a low side lobe level (<-20 dB), 20 dB gain, and a symmetric beam in the transverse plane was recently reported for real time *in situ* microwave measurement of material level at high temperatures.<sup>10</sup> A detailed analysis on the design, numerical optimization, and free space characterization of the corrugated horn for Gaussian beam was reported at room temperature in our prior work.<sup>10</sup> A high temperature sensor with a Gaussian (symmetric) beam was designed as industrial furnaces typically have ports with limited field of view and internal structures that can cause additional echoes which may potentially merge with the signal reflected by the target. Extensive measurements were carried out at room temperature for static and dynamically varying surfaces to quantify sensor accuracy and measurement stability for non-contact level measurement.<sup>10</sup> Preliminary measurement on the material level was reported for scrap metal inside a closed furnace to demonstrate the sensor suitability for high temperature applications.<sup>10</sup>

In this work, we present the signal analysis techniques for extracting thermodynamic phase change temperature of electric conducting and dielectric materials from the time gated *in situ* microwave reflections gathered by the air cooled corrugated horn reported in our earlier work.<sup>10</sup> Signal processing to compensate for the distortions introduced by discrete data sampling and band limited frequency domain measurements in the time domain is presented. Methodology for scaling and renormalization of the gated time domain reflection is presented to compensate for the effects of windowing in the processed frequency domain measurements. The proposed signal processing methodology is independent of the high temperature material. To validate the methodology, experiments were conducted for conductive (metal) and dielectric (glass) melts, and the information gathered from the processed microwave signals was verified with standard laboratory test and measurement techniques.

The organization of the paper is as follows: Sec. II presents the microwave measurement setup and high temperature materials used in this study. Section III presents the signal processing methodology to identify material thermodynamic phase change temperature from the microwave reflection measurements. Section IV presents the processed microwave frequency domain measurements for electrically conducting and dielectric materials and their comparison with conventional laboratory measurements. A summary of this work and comparison with other *in situ* sensors reported in the literature is covered in Sec. V. Section VI presents the conclusion.

## II. HIGH TEMPERATURE MEASUREMENT SETUP AND MATERIALS

### A. Measurement setup

Figure 1 shows the illustration of the experimental setup for *in situ* high temperature microwave material measurement

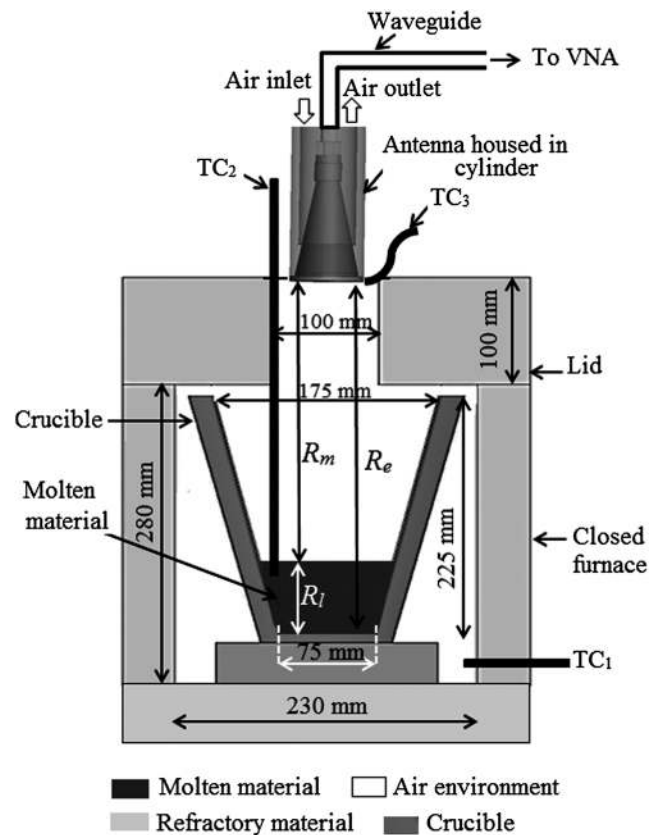


**FIG. 1.** High temperature non-contact *in situ* microwave material measurement setup. Cut view of the closed furnace illustrating sensor arrangement and positioning of the crucible and thermocouple sensors inside the closed furnace. Note: TC<sub>1</sub>, TC<sub>2</sub>, and TC<sub>3</sub> are K-type thermocouples connected to DAQ;  $R_e$ ,  $R_m$ , and  $R_l$  are the distance of the bottom of the empty crucible, material surface, and the level of the material inside the crucible measured with respect to the antenna aperture, respectively.

in a closed furnace with inner dimensions 230 mm × 230 mm × 280 mm and the location of the microwave antenna in the measurement setup. The sensor is a corrugated conical horn antenna with an aperture diameter of 52 mm fitted with a 3.7 mm thick quartz disc to avoid deposition of fine particles and vapor inside the antenna during *in situ* measurements in the furnace. The antenna was housed in a cylindrical hollow tube with provisions to circulate room temperature air (30 °C) for sensor cooling and maintain an air curtain in front of the quartz aperture to avoid particle and vapor deposition during *in situ* measurements in the furnace.

The continuous wave (CW) reflections from the crucible were gathered for discrete frequency steps over 20–24 GHz with −5 dBm transmitted power using a handheld VNA (N 9952A, Keysight Technologies, USA) remotely controlled by a computer. The furnace temperature and heating rate were controlled using a programmable controller. The temperature of the furnace, material inside the crucible, and antenna aperture were continuously recorded during measurement using K-type thermocouples (TC<sub>1</sub>, TC<sub>2</sub>, TC<sub>3</sub>) connected to the computer through a universal serial bus (USB) data acquisition board (DAQ) (NI 9211, National Instruments, USA).

## B. High temperature materials

Aluminum and glass were used for measuring the material thermodynamic phase change temperature from the microwave measurements. The solidified molten scrap metal in the crucible was used for measuring the melting point temperature ( $T_m$ ) of aluminum. Low sodium borosilicate glass beads with an average bead diameter of 2 mm were used to measure the glass transition ( $T_g$ ) temperature. The grain sizes (bead diameter) of the beads were between 1.7 mm and 2.36 mm and were verified using ASTM E11-70. The elemental composition of the materials was analyzed using the energy dispersive X-ray spectroscopy (EDS) technique (TEAM™ PEGASUS, EDS, USA). The melting point ( $T_m$ ) of aluminum and glass transition ( $T_g$ ) temperature of borosilicate glass were measured using the differential scanning calorimetry (DSC) technique. Simultaneous thermogravimetry (TG) and differential thermal analysis (DTA) of the material samples were carried out on a SEIKO instrument, Inc., EXSTAR TG/DTA 6300 analyzer. DSC measurements of specimens of about 10.5 mg were recorded using nitrogen as the purge gas (200 ml/min) at a heating rate of 10 °C/min with Al<sub>2</sub>O<sub>3</sub> (alumina) as a reference material.

### 1. Aluminum alloy

Table I shows the elemental composition of the aluminum alloy used in this work determined from EDS analysis. The composition indicates approximately 74% of aluminum and the presence of other elements in the metal alloy. Figure 2(a) shows the EDS spectrum of the aluminum alloy. The peaks indicate the intensity of the individual elements identified from energy dispersive X-ray analysis (EDAX). Figure 2(b) shows the DSC results of aluminum alloy. The intersection of the tangents near the peak in Fig. 2(b) indicates the material

TABLE I. Composition of aluminum alloy.

Element	Weight (%)
Chlorine (Cl)	0.31
Iron (Fe)	0.71
Oxygen (O)	5.79
Silicon (Si)	9.37
Carbon (C)	9.88
Aluminum (Al)	73.94

thermodynamic phase change temperature, i.e., melting point,  $T_m$  of the metal alloy, obtained from the DSC-TGA (thermogravimetric analysis) measurements. Due to the presence of other elements and impurities, the melting point of aluminum alloy was measured as 560 °C, which is lower than the pure metal (660 °C).<sup>11</sup>

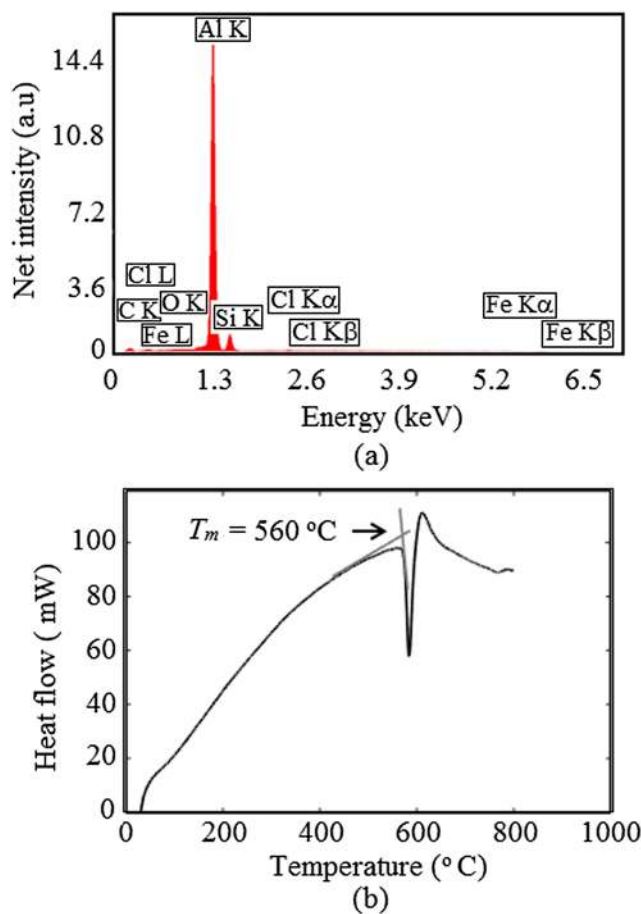


FIG. 2. Characterization of the aluminum alloy used for high temperature material measurement. (a) Elemental composition analyzed using the energy dispersive X-ray spectroscopy (EDS) technique and (b) differential scanning calorimetry (DSC) data of the alloy indicating the melting point temperature as 560 °C.

TABLE II. Composition of borosilicate glass.

Element	Weight (%)
Sulfur (S)	0.12
Titanium (Ti)	0.22
Iron (Fe)	0.28
Magnesium (Mg)	0.72
Aluminum (Al)	1.58
Silicon (Si)	6.88
Boron (B)	9.67
Sodium (Na)	10.11
Carbon (C)	18.44
Oxygen (O)	51.98

## 2. Borosilicate glass

Table II shows the glass composition obtained from EDAX measurements. Figure 3(a) shows the EDS spectrum, and

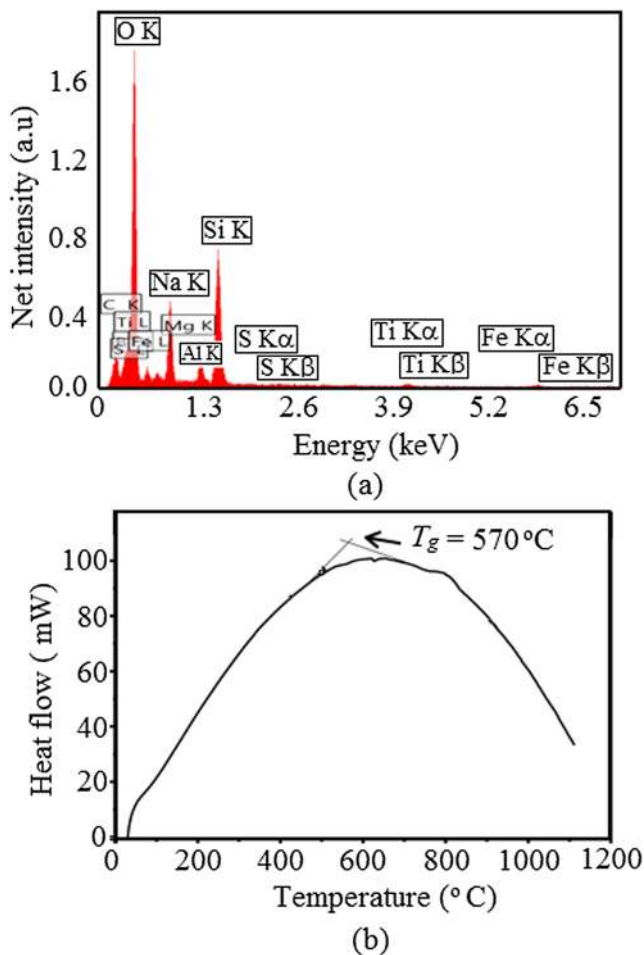


FIG. 3. Characterization of the borosilicate glass used for high temperature material measurement. (a) Elemental composition of borosilicate glass beads analyzed using the energy dispersive X-ray spectroscopy (EDS) technique and (b) differential scanning calorimetry (DSC) data of borosilicate glass beads indicating the glass transition temperature as 570 °C.

Fig. 3(b) shows the DSC result of the glass sample. Figure 3(b) indicates that the glass transition temperature,  $T_g$ , calculated by the tangent method is 570 °C.

## III. MICROWAVE SIGNAL ANALYSIS

The VNA provides the complex reflection coefficient,  $S_{11}(f)$ , at  $N$  discrete frequency points over the band limited frequency range defined by,  $f_1 \leq f \leq f_2$ , where  $f_1 = 20$  GHz and  $f_2 = 24$  GHz in this work. As Fourier transform operates on a continuous signal, inverse Fourier transform of the discrete band limited frequency domain data leads to issues in the time domain signal. Figure 4(a) shows the signal processing algorithms proposed to process the discrete band limited frequency domain CW reflection measurements for material property measurements without loss of information.

### A. Time domain transform of discrete band limited data

The band limited  $N$  point discrete frequency domain measurements,  $S_{11}(f)$ , have reflections from the antenna, measurement background, and crucible contents, i.e., material under test (MUT). Thus, the data were converted to time domain to identify the echo from the MUT and extract the associated frequency response. The discrete frequency domain measurement results in aliasing in time domain at a repeated time interval of  $1/\Delta f$ , where  $\Delta f$  is the uniform frequency step chosen in the measurement frequency range. Another issue with the discrete measurements is the truncated band limited data. The abrupt truncation is equivalent to multiplying the discrete infinitely extended frequency response of the measurement setup with a rectangular window spanning the frequency range,  $f_1 \leq f \leq f_2$ . This leads to ringing in time domain as the equivalent operation is convolution between the time domain transform of the infinitely extended discrete frequency response and a sine cardinal function. The issues with the time domain transform were compensated following steps (i)-(iv) in the signal processing flowchart shown in Fig. 4.

#### 1. Zero padding

The discrete band limited data were zero padded from  $f = 0$  to  $f_s$  at equally distributed frequency steps of  $\Delta f$ . Equation (1) shows the zero padded frequency response with  $M$  discrete points extending up to  $f = f_s$ , where  $f_s$  is the sampling frequency determined as per the Nyquist rate to avoid aliasing in the time domain,

$$S(f) = \begin{cases} 0, & 0 \leq f < f_1 \\ S_{11}(f), & f_1 \leq f \leq f_2 \\ 0, & f_2 < f \leq f_s \end{cases} \quad (1)$$

#### 2. Windowing and IFT

Inverse Fourier Transform (IFT) of the zero padded discrete frequency response,  $S(f)$ , leads to ringing in the time

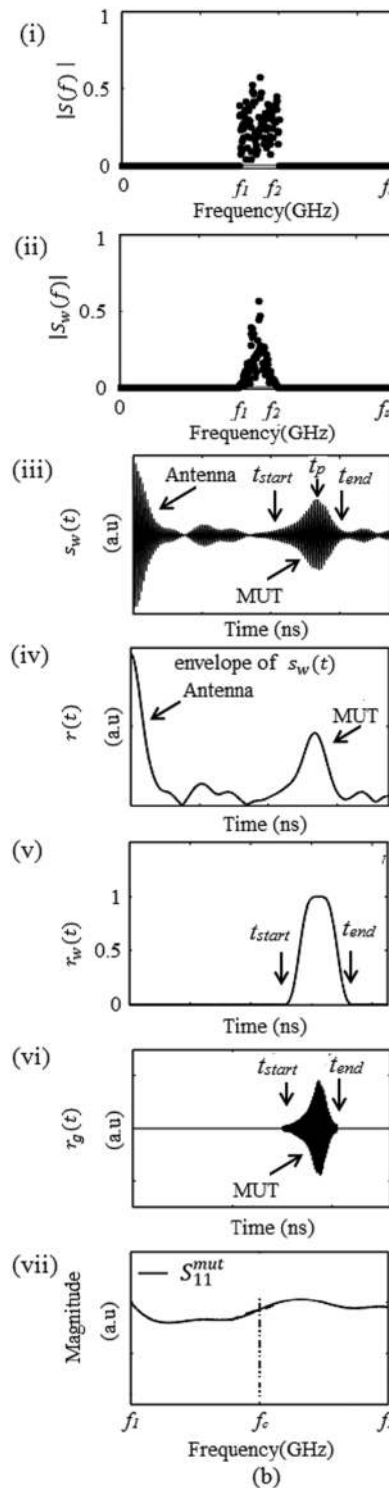
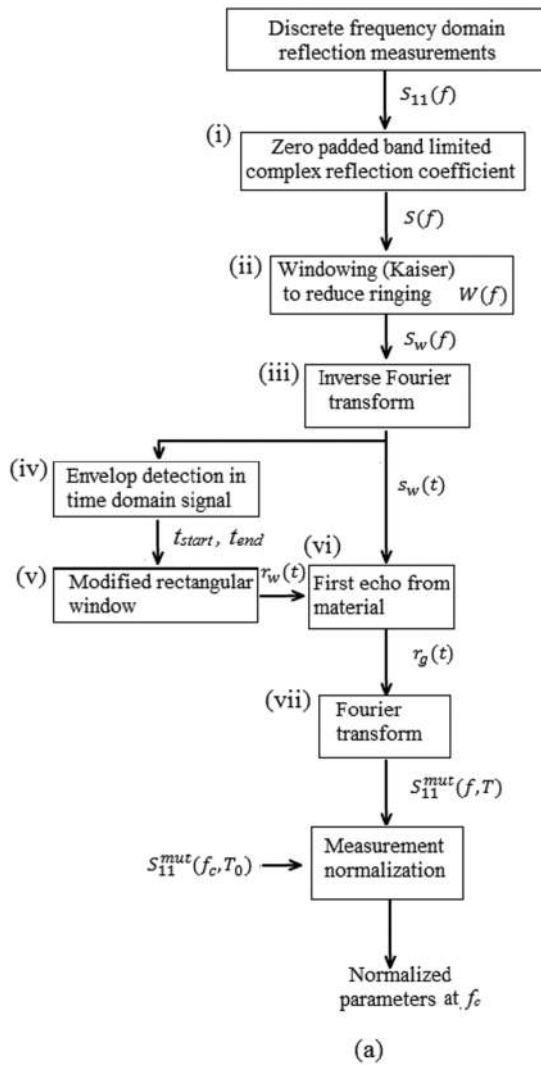


FIG. 4. Microwave signal analysis proposed for high temperature material property measurement. (a) Signal processing flowchart for analyzing the discrete and band limited frequency domain complex reflection measurements and (b) signals after each stage of the signal processing step proposed for *in situ* high temperature material measurement.

domain signal. The ringing caused by the truncation results in pulse broadening and reduces the ability to resolve the time of arrival of the reflections. Thus, a smooth windowing

function was applied to gradually reduce the frequency response to zero at  $f_1$  and  $f_2$  frequency points. A discrete Kaiser window function with finite support defined by

$$W_{11}(k) = I_0 \left[ \beta \sqrt{1 - \left( \frac{2k}{N-1} - 1 \right)^2} \right] / I_0[\beta], \quad -\left( \frac{N-1}{2} \right) \leq k \leq \left( \frac{N-1}{2} \right) \quad (2)$$

was used to smooth the discrete frequency response. In Eq. (2),  $I_0$  is the zeroth order modified Bessel function of the first kind and  $\beta$  controls the amplitude of the roll-off at the window start and end, i.e.,  $f_1$  and  $f_2$ , respectively. The  $N$  point discrete Kaiser window function in Eq. (2) with  $\beta = 6$  was chosen for the least ringing in time domain. The discrete window function was shifted to center frequency,  $f = f_c$ , and zero padded to a  $M$  point discrete frequency domain signal,

$$W(f) = \begin{cases} 0, & 0 \leq f < f_1 \\ W_{11}(f), & f_1 \leq f \leq f_2 \\ 0, & f_2 < f \leq f_s \end{cases} \quad (3)$$

The zero padded window function,  $W(f)$ , was multiplied point wise with  $S(f)$  to obtain the windowed discrete frequency response,  $S_w(f)$ . The IFT of  $S_w(f)$  yields an alias free signal,  $s_w(t)$  with reduced ringing in the time domain, where  $t$  denotes the time. The signal after each processing step is illustrated in Fig. 4(b).

## B. Envelope detection and echo location

The envelope of the  $M$  point time domain signal,  $s_w(t)$ , was obtained by applying Hilbert transform. The Hilbert transform of  $s_w(t)$  is a complex valued time domain signal given by

$$H\{s_w(t)\} = \frac{2}{\pi} \sum_{t=0}^{M-1} \frac{s_w(t)}{m-t}; \quad m = 0 \text{ to } M-1. \quad (4)$$

The magnitude of the Hilbert transform,

$$r(t) = |H\{s_w(t)\}|, \quad (5)$$

was used to obtain the envelope of the echoes in the time domain signal, as illustrated in Fig. 4(b). The maxima and minima identified in  $r(t)$  were fed to a peak search algorithm to identify the time of arrival of the echoes in the discrete time domain signal. The location of the peak corresponding to the reflections in the measurement setup is determined by converting the time axis to distance,  $d$ , using the conversion  $d = tc/2$ , where  $c$  is the wave velocity in the propagating medium which was set as free space velocity and the corresponding reflected signal be  $r(d)$ .

## C. Time gating and window renormalization

The objectives of time gating are to remove the stationary reflections present in the time domain signal,  $s_w(t)$ , due to impedance discontinuities in wave propagation arising from the antenna and crucible and retain the reflection from the MUT for further processing. Gating in time domain is performed to retain the reflection from the MUT defined over  $t_{start} \leq t \leq t_{end}$  centered at  $t = t_p$ , where  $t_p$  is the time corresponding to the peak of the first reflection from the

MUT extracted from the envelope signal,  $r(t)$ . The abrupt discontinuity in the gated time domain signal using a rectangular window function will lead to ringing in the frequency domain. Window re-normalization was implemented in this work to preserve the frequency content of the time gated reflection from the MUT using the following procedure: The signal corresponding to the first reflection from the MUT is time gated using a modified rectangular window function,

$$r_w(t) = w_R(t) * w_K(t), \quad (6)$$

with smooth support on either sides of the time window of interest,  $t_{start} \leq t \leq t_{end}$ , centered at  $t = t_p$ . In Eq. (6),  $w_R(t)$  and  $w_K(t)$  are the time shifted discrete rectangular and Kaiser ( $\beta = 6$ ) window functions, respectively, with finite support over  $[t_{start}, t_{end}]$  and  $*$  is the convolution operator. From Fig. 4(b), it can be observed that the modified window function,  $r_w(t)$ , has a flat top with a sharp roll-off at the support end points. This ensures that the frequency content of the gated signal is preserved with the least distortion when transformed to frequency domain. The Fourier transform of the time gated signal,

$$r_g(t) = s_w(t)r_w(t), \quad (7)$$

with the least distortion is used to extract the frequency response of the MUT,  $S_{11}^{mut}$ . The effect of windowing in time domain results in weighted response on either sides of the center frequency,  $f_c$ . Thus,  $S_{11}^{mut}$  at the center frequency,  $f = f_c$ , is used for measurement data analysis. The processed measurement,  $S_{11}^{mut}(f_c, T)$ , at a given temperature  $T$  is normalized with respect to its value at room temperature,  $S_{11}^{mut}(f_c, T_0)$ , to monitor the change in material reflection coefficient with respect to the material temperature.

Figure 5(a) shows the envelope of the reflections gathered by the antenna at room temperature for an empty crucible inside the furnace. The time axis was converted to distance in Fig. 5(a) for  $c = 3 \times 10^8$  m/s. The first maximum corresponds to wave reflection from the antenna-air interface ( $d = 0$ ). The second peak in Fig. 5(a) is due to the antenna internal reflections. The third peak is the wave reflection from the bottom surface of the empty crucible. The reflections from the furnace and the crucible wall are not present in the measurement [Fig. 5(a)] due to the low side lobe level and Gaussian beam pattern of the corrugated horn antenna. The distance between the antenna aperture and the crucible bottom,  $d = R_e$ , in Fig. 5(a) measured with respect to the antenna aperture is 360.1 mm compared to the physical distance of 360 mm. The difference in the distance between  $R_e$  and the peak of the reflection corresponding to the MUT, i.e.,  $d = R_m$ , was used to calculate the level,  $R_l = R_e - R_m$ , of the material inside the crucible. Figure 5(b) shows the unprocessed discrete band limited frequency domain reflection coefficients,  $S_{11}(f)$ , for the full measurement window (0–500 mm or 0–3.33 ns) shown in Fig. 5(a) and the processed frequency response,  $S_{11}^{mut}(f)$ , for the time gated reflection from the crucible bottom ( $R_e = 270$  to 450 mm or  $t = 1.8$  ns–3 ns) at room temperature,  $T = T_0$ .

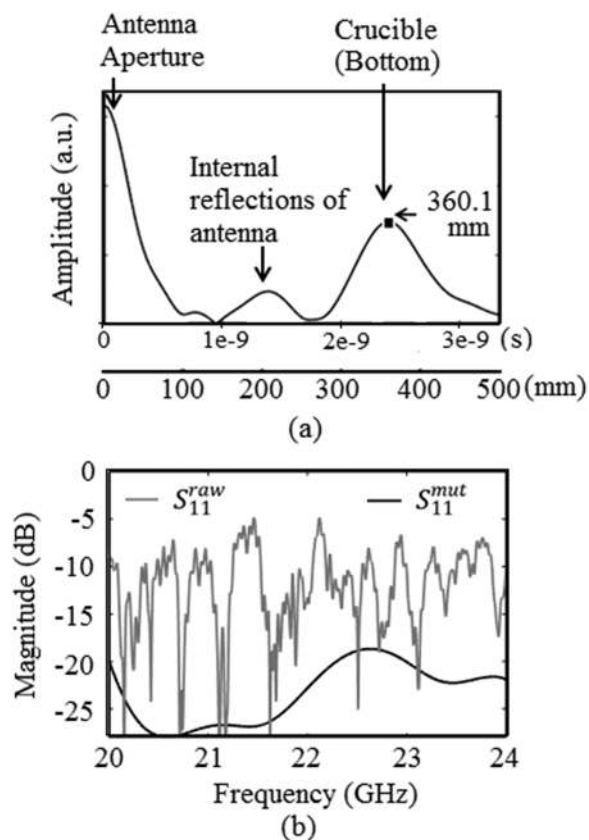


**FIG. 5.** Microwave measurements for an empty crucible at room temperature,  $T = T_0$ . (a) Envelope of the alias free discrete time domain signal,  $r(t)$ , and (b) magnitude of the truncated discrete frequency domain reflection coefficient before ( $S_{11}^{raw}$ ) and after ( $S_{11}^{mut}$ ) signal processing. Note:  $S_{11}^{mut}(f)$  is the frequency content of the time gated wave reflected from the crucible bottom, i.e.,  $r_g(t)$ .  $S_{11}(f)$  is the raw frequency data measured by the VNA for step frequency continuous wave (SFCW) excitation.

#### IV. HIGH TEMPERATURE MATERIAL MEASUREMENTS

##### A. Aluminum alloy

Figures 6(a) and 6(b) show the crucible with solidified MUT at room temperature and molten aluminum alloy, respectively. Figure 6(c) shows the temperature measurements of the furnace, MUT, and antenna aperture during *in situ* microwave measurements. From Fig. 6(c), it is clear that the furnace controller reached steady state temperature (TC<sub>1</sub>) of 1075 °C within 1.6 h ( $t = t_1$ ). The air cooled antenna aperture temperature (TC<sub>3</sub>) and MUT temperature (TC<sub>2</sub>) reached a steady state temperature of 390 °C and 700 °C, respectively, within 3.5 hours ( $t_3$ ) and continued at steady state for 4.3 h until the furnace was switched off ( $t = t_4$ ).

##### 1. Time gated reflection from MUT

Figure 7(a) shows the time series of the gated time domain signal,  $r_g(d)$ , processed from the SFCW reflection measurements recorded for 8 continuous hours for aluminum

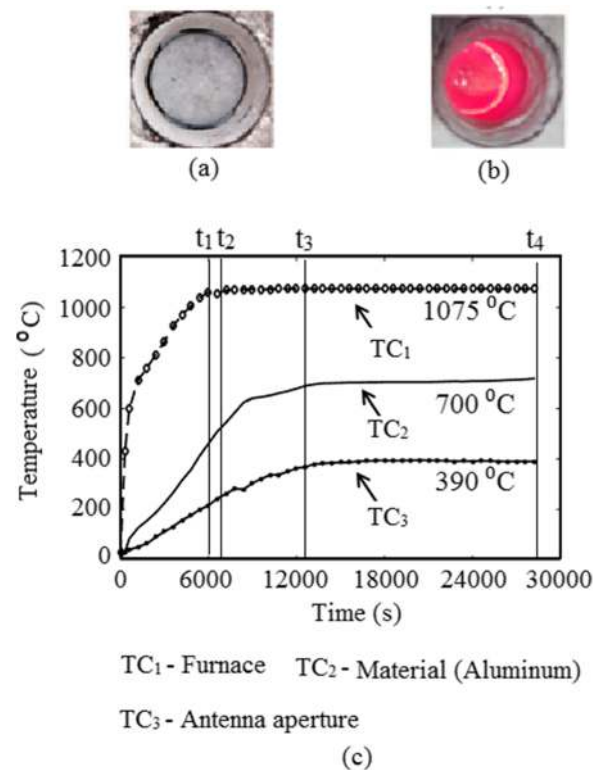


**FIG. 6.** High temperature processing of aluminum alloy inside a closed furnace. (a) Picture of the solidified aluminum alloy in the crucible at room temperature of 30 °C captured at time,  $t = 0$  s, (b) molten metal at the end of the heating study captured at time,  $t = t_4$  s, and (c) temperature profile inside the furnace during metal melting recorded by the *in situ* thermocouple sensors.

alloy during the metal melting process. The gated time domain signal in Fig. 7(a) corresponding to the wave reflected by the aluminum alloy indicates a decrease in signal amplitude with an increase in measurement time, in other words, an increase in material temperature. Figure 7(b) shows the absolute level of the metal ( $R_l$ ) inside the crucible extracted from the location of the peak,  $t = t_p$ , in Fig. 7(a). The small fluctuation in the material level inside the furnace observed in the beginning ( $t < t_3$ ) disappeared once the material reached steady state temperature, i.e.,  $t \geq t_3$ . The average level of the molten aluminum alloy ( $R_l$ ) was measured as 110.5 mm at the end of the heating study ( $t = t_4$ ). The level measured by a dip stick at time  $t = t_4$  was 110 mm.

##### 2. Melting point ( $T_m$ )

The time gated reflection coefficients,  $S_{11}^{mut}(f_c, T)$ , were extracted from the time domain signal,  $s_w(t)$ , following the procedure explained in Sec. III C. Figure 8 shows the relative change in the processed reflection coefficient of the MUT at 22 GHz ( $f_c$ ) with respect to room temperature measurement. Measurements are shown for two trials conducted on different days. From Fig. 8, it is clear that there is a sudden change in the normalized reflectivity at 545 °C for trial I and

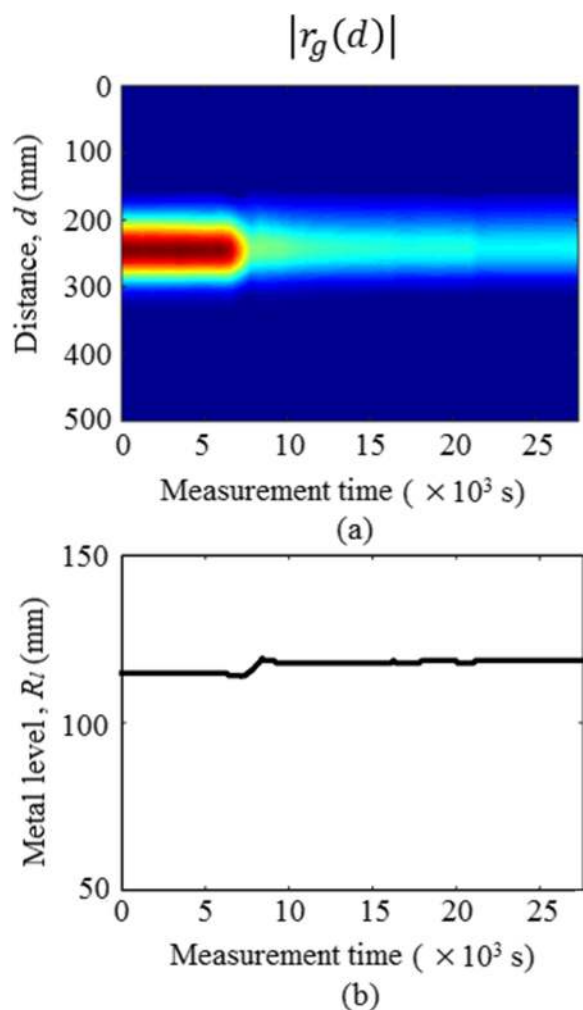


**FIG. 7.** Processed *in situ* microwave measurements for aluminum alloy recorded for 8 continuous hours inside a 1100 °C furnace. (a) Time series of the gated time domain signal,  $r_g(d)$  and (b) material level,  $R_l$ , extracted from the gated microwave measurements. The magnitude of the gated time domain signal decreased with an increase in material temperature with negligible variation in the level of the molten aluminum.

549 °C for trial II. The deflection occurred near the melting point of aluminum alloy ( $T_m$ ) which was measured as 560 °C in the DSC-TGA analysis.

The relative change in the reflectivity measurements observed in Fig. 8 is due to the change in the conductivity ( $\sigma$ ) of the metal alloy with respect to temperature. This phenomenon was confirmed using the low frequency resistivity measurements of pure aluminum (99.99%) reported in the literature.<sup>11</sup> The resistivity ( $\rho = 1/\sigma$ ) data reported by Desai *et al.* are consolidated measurements of different methods like potentiometer methods, AC-bridge, DC-bridge, heating method, and magnetic field methods at different temperatures.<sup>11</sup> Assuming plane wave interaction with the molten metal, the reflection coefficient for the layered 2D half space

Relative change in  $S_{11}^{mut}$  for aluminum alloy at  $f_c = 22$  GHz

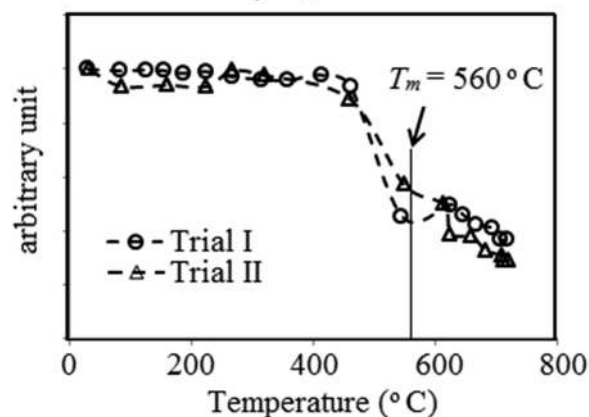


**FIG. 8.** Relative change in  $S_{11}^{mut}(f_c, T)$  of aluminum alloy at a center frequency of 22 GHz ( $f_c$ ) processed from the *in situ* microwave reflection measurements inside the closed furnace. The sudden change in the normalized reflectivity near the melting point,  $T_m$ , indicates the material state change from solid to liquid phase.

is given by<sup>12</sup>

$$\Gamma(f, T) = \frac{\eta(f, T) - \eta_0}{\eta(f, T) + \eta_0}. \quad (8)$$

In Eq. (8),  $\eta_0$  is the wave impedance in free space (377  $\Omega$ ) and  $\eta$  is the wave impedance of the metal<sup>11</sup> given by

$$\eta(f, T) = (1 + j)/\sigma\delta_s, \quad (9)$$

where  $\delta_s$  is the skin depth related to the material DC electrical conductivity ( $\sigma = 1/\rho$ ) and frequency of operation,  $f$ . It was shown by Desai *et al.* that resistivity of pure aluminum suddenly increased at the melting point (660 °C). Using Eqs. (8) and (9), it can be shown that the reflectivity of metal will decrease at  $T_m$ . Thus, the sudden change observed in Fig. 8 near the melting point ( $T_m = 560$  °C) indicates material thermodynamic phase change from solid to liquid state. It is well documented that the melting point<sup>13</sup> and conductivity<sup>14</sup> of metal alloys are influenced by their elemental composition. Thus, the material thermodynamic phase change identified from the processed microwave measurements occurred at a lower temperature of 560 °C which is the melting point of the aluminum alloy as verified from DSC-TGA data (Fig. 2).

## B. Borosilicate glass

Figure 9(a) shows the crucible with the glass beads used in this study. Figure 9(b) shows the glass melt at the end of the experiment. Figure 9(c) shows the temperature profile of the furnace, glass, and antenna aperture recorded during the glass melting process. In Fig. 9(c), the furnace controller reached a steady state temperature ( $TC_1$ ) of 1075 °C within 1.3 h ( $t_1$ ). The air cooled antenna aperture ( $TC_3$ ) and glass ( $TC_2$ ) reached a steady state of 400 °C and 725 °C, respectively, within first

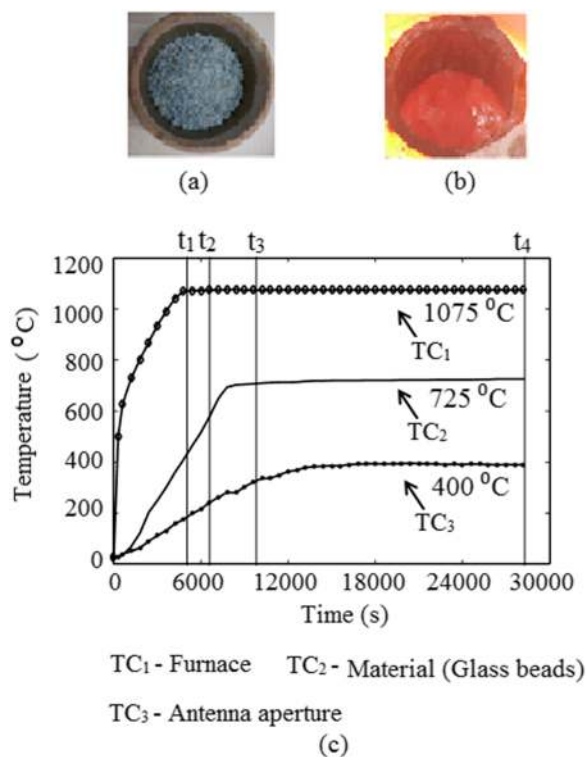


**FIG. 9.** High temperature processing of borosilicate glass beads in a closed furnace. (a) Picture of the glass beads in the crucible at room temperature of 30 °C captured at time  $t = 0$  s, (b) molten glass at the end of the heating study captured at time  $t = t_4$  s, and (c) temperature profile inside the furnace during glass melting recorded by using the *in situ* thermocouple sensors.

3 h ( $t_3$ ) and remained at steady state for 4.8 h until the furnace was switched off ( $t_4$ ). Figure 9(c) confirms that the glass was in the molten state for time  $t \geq t_3$ .

### 1. Time gated reflection from MUT

Figure 10(a) shows the time series of the gated time domain data,  $r_g(d)$ , processed from the *in situ* microwave reflection measurements,  $S_{11}(f)$ , of borosilicate glass recorded inside the closed furnace. Figure 10(b) shows the average level of glass ( $R_l$ ) in the crucible during the melting process extracted from the signal peak of  $r_g(d)$ . Large variation in the location of the reflected signal peak from the MUT,  $R_l$ , was observed in the beginning ( $t < t_2$ ) due to the release of air bubbles trapped in between the glass beads. The fluctuations in the glass surface ( $R_m$ ) disappeared as the glass temperature increased more than the  $T_g$  measured in DSC-TGA analysis. The average level of the glass melt,  $R_l$ , inside the crucible was measured as 35.7 mm for  $t > t_3$  which agreed with the dip stick measurement of 35 mm recorded at the end of the heating study ( $t = t_4$ ).

### 2. Glass transition temperature ( $T_g$ )

Figure 11 shows the normalized time gated reflection coefficient,  $S_{11}^{mut}(f_c, T)$ , of borosilicate glass extracted from the

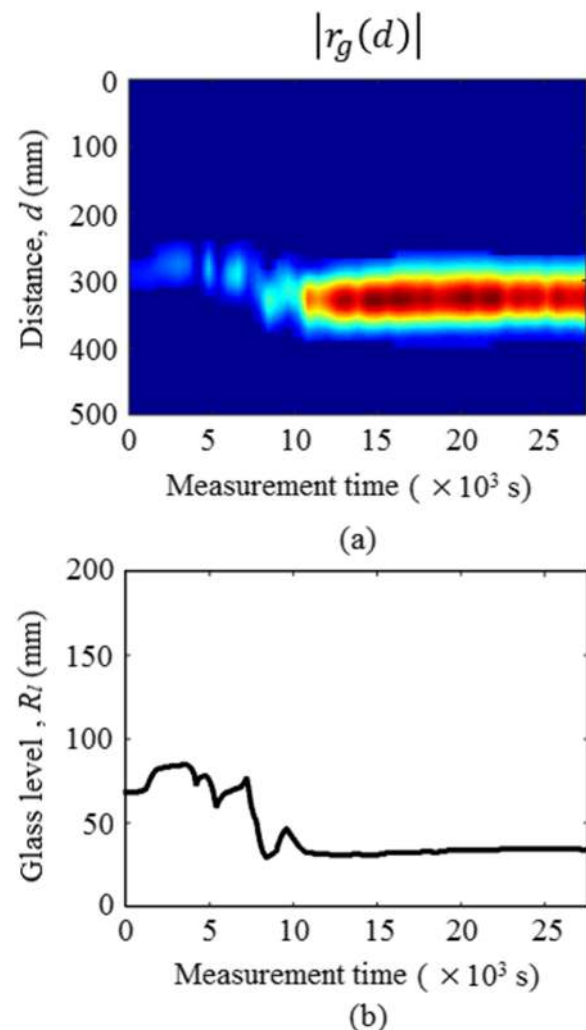


**FIG. 10.** Processed *in situ* microwave measurements of borosilicate glass recorded for 8 continuous hours inside the 1100 °C furnace. (a) Time series of the gated time domain signal,  $r_g(d)$ , and (b) material level,  $R_l$ , extracted from the gated microwave measurements. The magnitude of the gated time domain signal increased with an increase in material temperature with negligible variation in the level of the molten glass at the end of the 8 h heating study.

*in situ* microwave reflection measurements,  $S_{11}(f)$ , recorded during the melting process. From Fig. 11, it is clear that there is an abrupt change in the reflected field strength at 566 °C for trial I and 574 °C for trial II. The glass transition temperature of glass matrices occurs before crystallization and melting processes.<sup>15</sup> Thus, based on DSC-TGA analysis, the observed change in the processed reflection measurements was identified as the glass transition temperature ( $T_g$ ) for two trials carried out on different days.

Unlike metals, the conductivity of glass matrices increases with an increase in temperature.<sup>16-18</sup> Glass conductivity measurements reported by Maji *et al.*<sup>17</sup> indicated that the electrical conductivity ( $\sigma$ ) of borosilicate glass suddenly increased

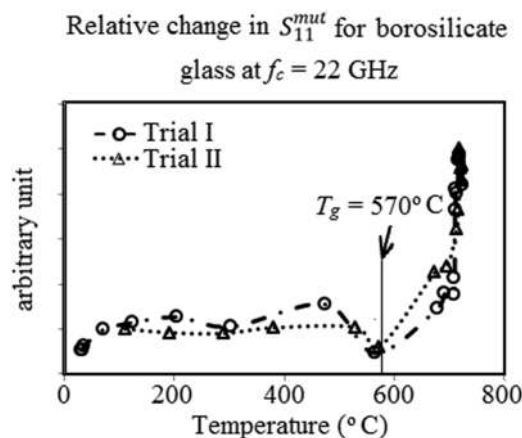


**FIG. 11.** Relative change in  $S_{11}^{mut}(f_c, T)$  of borosilicate glass at a center frequency of 22 GHz ( $f_c$ ) processed from the *in situ* microwave reflection measurements inside the closed furnace. The sudden increase in the normalized reflectivity near the melting point,  $T_m$ , indicates the material state change from solid to liquid phase.

at 530 °C which was reported as the glass transition temperature for the analyzed glass matrix composition. The wave impedance of a dielectric material such as glass is related to its electrical conductivity by<sup>12</sup>

$$\eta = \frac{j\omega\mu}{\gamma}, \quad (10)$$

where  $\gamma = \sqrt{j\omega\mu\sigma - \omega^2\mu\epsilon}$  is the complex wave propagation constant,  $\mu$  is the magnetic permeability of the glass matrix,

and  $\omega$  is the angular frequency. It is also reported that the variation in the dielectric constant of the borosilicate glass matrix with temperature is relatively small.<sup>19</sup> From Eqs. (8) and (10), and the literature on high temperature measurements of glass, it is concluded that the reflectivity ( $\Gamma$ ) of borosilicate glass is significantly influenced by the conductivity ( $\sigma$ ) variation with temperature. Thus, it was concluded that the abrupt change in Fig. 11 denotes  $T_g$  of the glass matrix. The glass transition temperature identified from the time gated processed microwave measurements agreed with the DSC-TGA measurement ( $T_g = 570$  °C) shown in Fig. 3(b).

## V. SUMMARY

Several studies are reported in the literature for coupon level measurement of high temperature material properties. Such laboratory scale measurement techniques are not suited for industrial furnaces. Very few studies are reported for bulk material measurements in industrial scale furnace using electromagnetic waves. The most relevant ones are the work reported by Woskov *et al.*<sup>3</sup> and Pieraccini *et al.*<sup>4</sup> The contact type millimeter wave measurement technique reported by Woskov *et al.* needs frequent replacement of the sensor due to material and vapour deposition inside the sensor and has a poor signal to noise ratio. The non-contact microwave based active measurement technique reported by Pieraccini *et al.* uses the interferometry principle for measuring only the change in the level of molten glass. Furthermore, this technique gives ambiguous measurement when the change in the material level is more than one half of the wavelength. In this work, we have used a compact (52 mm diameter) air cooled

**TABLE III.** Comparison of *in situ* methods proposed for high temperature process parameter measurement inside the furnace.

Particulars	Methods			
	Thermocouple <sup>20</sup>	Ultrasound	Microwave/millimeter wave	This work
Material parameters	<ul style="list-style-type: none"> <li>Absolute level</li> <li>Temperature</li> </ul>	<ul style="list-style-type: none"> <li>Absolute level<sup>1</sup></li> <li>Mechanical properties<sup>5</sup></li> </ul>	<ul style="list-style-type: none"> <li>Level change<sup>4</sup></li> <li>Temperature, emissivity, and density<sup>3</sup></li> <li>Absolute level<sup>9</sup></li> </ul>	<ul style="list-style-type: none"> <li>Absolute level</li> <li>Melting point</li> <li>Glass transition temperature</li> </ul>
Non-contact	No	No <sup>1,5</sup>	No, <sup>3</sup> yes <sup>4,9</sup>	Yes
Sensing element	Linear thermocouple array inside a thermowell	Waveguide <sup>5</sup>	Dielectric waveguide <sup>3</sup> and conical horn antenna <sup>4</sup> Dielectric rod antenna <sup>9</sup>	Corrugated horn antenna
Working principle	Resistance change in metal junction	Time of flight of reflected wave	Passive MMW radiation <sup>3</sup> and phase of SFCW reflection <sup>4</sup> Complex SFCW reflection <sup>9</sup>	Complex SFCW reflection
Furnace temperature	890–1350 °C	246 °C, <sup>1</sup> 1200 °C <sup>5</sup>	1200 °C <sup>3</sup> 1300 °C <sup>4</sup> Not demonstrated <sup>9</sup>	1100 °C
Measurement range inside the furnace	Depends on array configuration	Range: determined by waveguide length <sup>1</sup> Level: 0.3% accuracy <sup>1</sup>	Not applicable. <sup>3,a</sup> Minimum range: 0.5 m <sup>4</sup> Level change: 0.5 mm accuracy <sup>4</sup> Not demonstrated <sup>9</sup>	Minimum range: 0.25 m <sup>10</sup> Level: 0.1 mm accuracy

<sup>a</sup>Range is not applicable for this contact type waveguide sensor.<sup>3</sup>

(ambient air) corrugated horn for non-contact active measurement at a very low power level ( $-5$  dBm). The proposed sensor has a higher signal to noise ratio as it is operated in active mode, and it was not influenced by vapor deposition due to the existence of the air curtain on the quartz disc. Furthermore, the signal processing algorithms use both magnitude and phase information of the reflected signal to identify the absolute location of the material and extract the signal variation for the material at high temperatures. *In situ* microwave material measurements using a compact sensor with better radiation characteristics and signal processing algorithms for the complex reflection measurements to extract material thermodynamic phase change temperature are the contributions of this work. The robustness of the proposed microwave measurement technique was demonstrated for electrically conducting (metal) and insulating (glass) materials. The abrupt variation in the processed signals observed at high temperatures coincided with the material thermodynamic phase change temperature, i.e., melting point ( $T_m$ ) of aluminum alloy and glass transition temperature ( $T_g$ ) of borosilicate glass. Currently, non-contact measurement of material thermodynamic phase change in furnace is only possible using a pyrometer. A comparison of the microwave high temperature material measurement technique reported in this work with other similar studies in the literature is summarized in Table III. From Table III, it can be concluded that the proposed non-contact microwave technique is capable of measuring the absolute level and thermodynamic phase change temperature of the material when compared to other non-contact measurement techniques that yield either an absolute or relative level.

## VI. CONCLUSION

A non-contact microwave sensor is presented for real time continuous high temperature process monitoring of metals and non-metals in a closed furnace. The signal processing algorithms implemented to process the *in situ* microwave reflection measurements were presented in detail. Continuous *in situ* recording of the wave reflections,  $S_{11}(f, T)$ , during high temperature material processing, and monitoring the change in the processed wave reflection coefficient,  $S_{11}^{mut}(f_c, T)$ , with respect to the room temperature measurement,  $S_{11}^{mut}(f_c, T_0)$ , yielded non-contact determination of the thermodynamic phase change temperature during high temperature material processing. The proposed non-contact *in situ* microwave measurement method and signal processing techniques for real time measurement of the thermodynamic phase change temperature were experimentally validated for metal alloy and borosilicate glass widely used in

manufacturing industries. The processed microwave high temperature material measurements reported for metal alloy and glass are repeatable and in good agreement with the measurements obtained using conventional methods.

## ACKNOWLEDGMENTS

The authors thank Dr. M. Balachary, Associate Director of Defence Electronics Research Laboratory (DLRL), Hyderabad, India, for antenna pattern measurements, Professor Jayaganthan, Department of Engineering Design, Indian Institute of Technology (IIT) Madras for DSC measurements, Dr. G. Balaganesan, Central Workshop, IIT Madras for providing access to the furnace, and Keysight Technologies, India, for their support with the RF analyzer. This work was supported by the DAE, Board of Research in Nuclear Science (BRNS), Government of India.

## REFERENCES

- 1 L. S. Boehmer and R. W. Smith, *IEEE Trans. Nucl. Sci.* **23**, 359 (1976).
- 2 T. Ihara, N. Tsuzuki, and H. Kikura, *Prog. Nucl. Energy* **48**, 90 (2016).
- 3 P. Woskov, *International Conference Infrared and Millimetre Wave* (IEEE, San Diego, CA, USA, 2002), p. 13.
- 4 M. Pieraccini, D. Mecatti, D. Dei, F. Parrini, G. Macaluso, A. Spinetti, and F. Puccioni, *Sensors Act. A, Phys.* **212**, 52 (2014).
- 5 S. Periyannan and K. Balasubramaniam, *Rev. Sci. Instrum.* **86**, 114903 (2015).
- 6 E. Blomme, D. Bulcan, and F. Declercq, *NDT&E Int.* **35**, 417 (2002).
- 7 R. Zhoughi, *Microwave Non-Destructive Testing and Evaluation* (Kluwer Academic Publishers, The Netherlands, 2012).
- 8 C. A. Balanis, *Antenna Theory: Analysis and Design*, 3rd ed. (Wiley, New Jersey, 2005).
- 9 G. Armbrecht, C. Zietz, E. Denicke, and I. Rofles, *IEEE Trans. Antennas Propag.* **60**, 5083 (2012).
- 10 B. T. Sivaprakasam, C. V. Krishnamurthy, and K. Arunachalam, *IEEE Sensors J.* **18**, 4081 (2018).
- 11 P. D. Desai, H. M. James, and C. Y. Ho, *J. Phys. Chem. Ref. Data* **13**, 1131 (1984).
- 12 D. M. Pozar, *Microwave Engineering*, 3rd ed. (Wiley, New Delhi, 2007).
- 13 J. R. Davis, *Alloying: Understanding the Basics* (ASM Int., 2001), p. 651.
- 14 M. Mujahid and N. N. Engel, *Scr. Metall.* **13**, 887 (1979).
- 15 L. D. Pye, A. Montenero, and I. Joseph, *Properties of Glass-Forming Melts* (CRC Press, Boca Raton, 2005).
- 16 C. L. Babcock, *J. Am. Ceram. Soc.* **17**, 329 (1934).
- 17 B. K. Maji, H. Jena, and R. Asumvathraman, *J. Non-Cryst. Solids* **434**, 102 (2016).
- 18 Q. Zheng, J. C. Mauro, M. M. Smedskjaer, R. E. Youngman, M. Potuzak and Y. Yue, *J. Non-Cryst. Solids* **358**, 658 (2016).
- 19 D. Krause and H. Bach, *Schott Series on Glass and Glass Ceramics Science, Technology, and Applications* (Springer-Verlag Berlin and Heidelberg GmbH & Co. Kg, Germany, DE, 1995–2005).
- 20 See <https://br.omega.com> for Super OMEGACLAD® XL Thermocouple Probes Data Sheet (last accessed February 07, 2019).